

Array-CGH Reveals Recurrent Genomic Changes in Merkel Cell Carcinoma Including Amplification of L-Myc

Kelly G. Paulson^{1,2,15}, Bianca D. Lemos^{1,2,15}, Bin Feng³, Natalia Jaimes⁴, Pablo F. Peñas⁵, Xiaohui Bi⁶, Elizabeth Maher⁷, Lisa Cohen^{8,9}, J. Helen Leonard¹⁰, Scott R. Granter^{11,12}, Lynda Chin^{13,14} and Paul Nghiem^{1,2}

Merkel cell carcinoma (MCC) is an aggressive neuroendocrine skin cancer with poorly characterized genetics. We performed high resolution comparative genomic hybridization on 25 MCC specimens using a high-density oligonucleotide microarray. Tumors frequently carried extra copies of chromosomes 1, 3q, 5p, and 6 and lost chromosomes 3p, 4, 5q, 7, 10, and 13. MCC tumors with less genomic aberration were associated with improved survival ($P=0.04$). Tumors from 13 of 22 MCC patients had detectable Merkel cell polyomavirus DNA, and these tumors had fewer genomic deletions. Three regions of genomic alteration were of particular interest: a deletion of 5q12-21 occurred in 26% of tumors, a deletion of 13q14-21 was recurrent in 26% of tumors and contains the well-characterized tumor suppressor RB1, and a previously unreported focal amplification at 1p34 was present in 39% of tumors and centers on L-Myc (MYCL1). L-Myc is related to the c-Myc proto-oncogene, has transforming activity, and is amplified in the closely related small cell lung cancer. Normal skin showed no L-Myc expression, whereas 4/4 MCC specimens tested expressed L-Myc RNA in relative proportion to the DNA copy number gain. These findings suggest several genes that may contribute to MCC pathogenesis, most notably L-Myc.

Journal of Investigative Dermatology advance online publication, 20 November 2008; doi:10.1038/jid.2008.365

INTRODUCTION

Merkel cell carcinoma (MCC) is a neuroendocrine cancer of the skin. It is believed to arise from the sensory Merkel cells normally found in the lower epidermis and hair follicles (Haeberle *et al.*, 2004; Boulais and Misery, 2007). Clinically,

MCC typically presents as a rapidly growing, painless, red nodule on sun-exposed skin and carries a poor prognosis (Heath *et al.*, 2008). Indeed, MCC is lethal in 33% of cases (Hodgson, 2005) and thus has a worse prognosis than that of melanoma (American Cancer Society, 2006). Improved diagnostic techniques and an aging population have contributed to a rapid rise in the reported incidence; currently 1,500 new cases of MCC are diagnosed annually in the United States (Lemos and Nghiem, 2007).

The key oncogenic events in MCC are not well understood. Recently, a search for unique cDNA sequences present in MCC identified a previously unreported polyomavirus that was present in 8 of 10 tumor samples (Feng *et al.*, 2008). Although existing data suggest that this virus is neither necessary nor sufficient for developing MCC, it is an open question as to whether the virus contributes to carcinogenesis in a subset of cases.

Forays into several major cancer pathways including p53 (Van Gele *et al.*, 2000), Wnt (Liu *et al.*, 2007), c-Kit (Swick *et al.*, 2007), BRAF, and other MAP kinase pathway members (Houben *et al.*, 2006) have revealed little involvement of these canonical cancer pathways in the pathogenesis of MCC. The generally null findings of these directed investigations highlight the need for an unbiased approach to identify candidate oncogenic pathways for further exploration.

Comparative genomic hybridization (CGH) is a technique used to map regions of copy number alteration in a cancer genome. CGH compares DNA derived from cancer cells to

¹Department of Medicine, University of Washington, Seattle, Washington, USA; ²Department of Dermatology, University of Washington, Seattle, Washington, USA; ³Dana-Farber Cancer Institute, Boston, Massachusetts, USA; ⁴Universidad Pontificia Bolivariana, Medellín, Colombia; ⁵Westmead Hospital, University of Sydney, Sydney, Australia; ⁶University Hospital Cancer Center, University of Medicine and Dentistry, Newark, New Jersey, USA; ⁷University of Texas Southwestern Medical Center, Dallas, Texas, USA; ⁸Caris Cohen Dx, Newton, Massachusetts, USA; ⁹Tufts University School of Medicine, Boston, Massachusetts, USA; ¹⁰Neuroendocrine Biology Group, Queensland Institute of Medical Research, Brisbane, Queensland, Australia; ¹¹Department of Pathology, Brigham and Women's Hospital, Boston, Massachusetts, USA; ¹²Harvard Medical School, Boston, Massachusetts, USA; ¹³Department of Medical Oncology, Dana-Farber Cancer Institute, Boston, Massachusetts, USA and ¹⁴Department of Medicine, Harvard Medical School, Boston, Massachusetts, USA

¹⁵These authors contributed equally to this work.

This work was performed in Boston, MA, USA, and Seattle, WA, USA.

Correspondence: Dr Paul Nghiem, Department of Medicine/Dermatology, University of Washington, 815 Mercer Street, Seattle, Washington 98109, USA.

E-mail: pngnhiem@u.washington.edu

Abbreviations: CGH, comparative genomic hybridization; FFPE, formalin-fixed paraffin embedded; MCC, Merkel cell carcinoma; MCPyV, Merkel cell polyomavirus; SCLC, small cell lung cancer

Received 13 March 2008; revised 5 September 2008; accepted 10 September 2008

normal diploid DNA to detect copy number imbalance in cancer cells. Classical chromosome CGH relies on light microscopy of metaphase spreads and resolution is thus limited. Several studies have used chromosome CGH in MCC (Harle *et al.*, 1996; Van Gele *et al.*, 1998, 2002; Popp *et al.*, 2002; Larramendy *et al.*, 2004) but did not have sufficient resolution to delineate specific candidate oncogenes or tumor suppressors. Modern array-CGH technology on oligonucleotide microarrays improves resolution up to a thousand fold and can define copy number alterations in regions as small as a single gene (Brennan *et al.*, 2004). Array-CGH has been employed successfully to profile genetic aberrations and identify cancer-relevant genes in many malignancies such as lung and pancreatic cancer (Aguirre *et al.*, 2004; Tonon *et al.*, 2005).

We performed array-CGH on 25 MCC tumor samples using a DNA-microarray imprinted with >40,000 oligonucleotides that spanned the genome with a distance of only 24 kb between probes in gene rich regions. This greatly improved resolution has allowed identification of several focal regions of aberration containing candidate genes for further investigation in MCC pathogenesis.

RESULTS

Patient and tumor characteristics

We studied 28 MCC tumor specimens from 25 patients with MCC. Our samples were a mixture of formalin-fixed paraffin-embedded (FFPE) tumors and flash-frozen tumors. Data were excluded from three FFPE specimens because of high noise; analysis continued with the remaining 25 samples from 23

Table 1. Patient and tumor characteristics

Sample ID	Sample type	Site of primary tumor	Size of primary tumor (cm)	Sex	Age	Disease course and comments	% Probes aberrant (>2.3n or <1.75n)	MCPyV detected?
MCCd1p	Primary*	Head/neck	1.1	F	79	Died of disease at 14 months	20	Y
MCCd1m	Metastasis of MCCd1p*	Head/neck	1.1	F	79	Died of disease at 14 months	17	Y
MCCd3p	Primary*	Buttock	6	M	45	Died of disease at 22 months; HIV+	15	Y
MCCd3m	Metastasis of MCCd3p*	Buttock	6	M	45	Died of disease at 22 months; HIV+	10	Y
MCCd5	Primary*	Upper limb	5.2	M	63	No relapse at 14 months	3	N
MCCd6	Primary*	Lower limb	2.3	M	50	No relapse at >36 months	6	Y
MCCd7	Node*	Upper limb	0.6	F	76	No relapse at >36 months	4	Y
MCCd8	Primary*	Head/neck	2.2	F	86		16	Y
MCCd9	Primary*	Upper limb	1	F	69		3	Y
MCCd10	Primary*	Flank	1.2	M	86	Patient on immunosuppressives	40	Y
MCCd11	Primary*	Upper limb	1.7	F	85	Collision tumor with squamous-cell carcinoma	58	Y
MCCd12	Primary*	Lower limb	1.3	M	85	Died disease free at 16 months; also had renal cancer	2	Y
MCCd13	Metastasis*	Lower limb	2	M	80	Alive with disease at 6 months; NED at 30 months (regression)	13	Y
MCCd14	Primary*	Lower limb	2.5	M	47	Alive with disease at 5 months; still alive at 24 months	11	Y
MCCd15	Primary*	Chest	0.5	M	73	No relapse at 5 months	6	
MCCd16	Primary*	Upper limb	1.6	M	72	No relapse at 10 months; patient has bladder cancer	63	N
MCC ₁ T	Node	Head/neck	0.6	F	63	Died of disease at 14 months	29	N
MCC ₁ 3T	Node		0.2	M	68	No relapse at >36 months	35	N
MCC ₁ 4T	Node	Head/neck		M	77	Died of disease at 40 months	24	N
MCC ₁ 5T	Recurrence	Head/neck		F	72	Died of disease at 26 months	65	N
MCC ₁ 12T	Recurrence	Head/neck	3	M	61	Died of disease at 9 months	21	N
MCC ₁ 13T	Node	Head/neck	0.6	F	65	No relapse at >36 months	3	Y
MCC ₁ 16T	Recurrence	Head/neck	0.7	M	71		20	N
MCC ₁ 21T	Node	Lower limb		M	82	Alive with disease at 33 months	10	Y
MCC ₁ Sm	Primary	Head/neck		M	70		22	N

MCPyV; Merkel cell polyomavirus, presence detected by PCR; NED; No evidence of disease. Asterisks (*) represent formalin-fixed paraffin embedded specimens; all other DNA was extracted from flash-frozen tumors. Times are reported as time since diagnosis. Data were not available for cells that remain empty.

patients. Most specimens contained over 90% tumor cells, and all specimens contained at least 70% MCC tumor cells.

The patients in this cohort were similar to prior reports with regard to demographics (Table 1) as the average age at diagnosis was 71 years, and 65% (15/23) were men (Allen *et al.*, 2005; Heath *et al.*, 2008). Thirteen primary tumors, six lymph node metastases, three distant metastases, and three recurrences were studied. Primary tumor size information was available for 12 of 13 primary tumors studied. In these tumors, the diameter ranged between 0.5 and 6 cm, and the median tumor size was 1.65 cm. Interestingly, we observed no relationship between primary tumor size and extent of copy number alteration (data not shown). The study included a heterogeneous group of samples including primary, recurrent, nodal metastatic, and distant metastatic tissues. However, for the patients for which both a primary and metastasis were profiled, the signatures were nearly identical between the primary and metastasis, suggesting that heterogeneity of the sample types does not substantially affect interpretation of the data.

Eight of the 25 specimens reported here had been previously studied using classical CGH approaches (metaphase spreads). Specimens MCC_L1T, MCC_L3T, MCC_L4T, MCC_L5T, MCC_L12T, MCC_L13T, MCC_L16T, and MCC_L21T were previously reported as MCC1, MCC3, MCC4, MCC5, MCC12, MCC13, MCC16, and MCC21, respectively (Van Gele *et al.*, 1998). An "L" is added to the original sample names to avoid confusion with other samples in this study labeled "d." These samples were included in this study because the array-CGH improves resolution of copy number alteration allowing detection of previously unseen regions of alteration.

Detection of the Merkel cell polyomavirus

Specimens were tested for the presence or absence of Merkel cell polyomavirus (MCPyV or MCV) DNA by real-time PCR, as described (Garneski *et al.*, 2008b), and virus was detected in tumors from 13 of 22 patients (59%; Table 1). We cannot exclude the possible presence of a strain variant in samples with no detectable MCPyV. Comparing virus positive MCC to MCC with no detectable virus, there was a trend (not

significant) towards less aberration in virus positive tumors, especially for regions of deletion (Supplementary Materials, Figure S1).

Array-CGH detects focal changes in DNA copy number in MCC tumors

Genome-wide array-CGH was performed on genomic DNA extracted from both frozen and FFPE tissues. Although noise tended to be greater with FFPE samples, sufficient signals were detectable in most cases (Figure 1). For each sample, a graphical plot and the associated raw numerical data are included in Supplementary Materials (Figure S2).

Recurrent genomic changes across MCC tumors

Analysis of copy errors detection was used to identify regions of copy number aberration for each MCC specimen (see Materials and Methods section). To determine recurrent regions of aberration, we combined the data from 23 MCC specimens (only the primary was included for the two patients with both primary and metastatic tissue analyzed). For each probe, the percentage of MCC tumors that were amplified or deleted was calculated (Figure 2). Magnitude of aberration was not considered so long as the software determined the change in copy number to be statistically significant. A stringent cutoff was used to favor detection of high amplitude events that are less likely to be technical noises (see Materials and Methods section).

Chromosomes 1, 3q, 5p, and 6 were most frequently increased in copy number whereas chromosomes 3p, 4, 5q, 7, 10, and 13 were most frequently lost. These global findings concur with those previously published for MCC using classical CGH (Harle *et al.*, 1996; Van Gele *et al.*, 1998, 2002; Popp *et al.*, 2002; Larramendy *et al.*, 2004). We also performed recurrence analysis including only samples not previously studied and found the genome-wide results to be very similar (data not shown).

Low levels of genomic change were associated with improved prognosis

To estimate the amount of overall genomic alteration per sample, we called probes as aberrant if they had analysis of

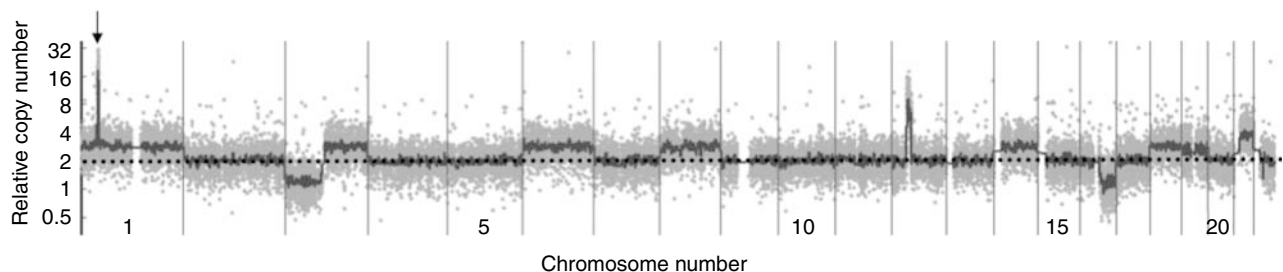


Figure 1. Genome-wide profile of a representative MCC tumor. Genome-wide overview of array-CGH data that graphically depicts changes in copy number for sample MCCd10. On the x-axis (dotted line) data points are organized along the 22 autosomal chromosomes arranged from largest (on left) to smallest. A dotted line is shown at the level of $2n$ (normal) relative DNA amount and the y-axis depicts relative copy number on a logarithmic scale. Light gray dots represent individual data points, and the dark gray line represents the line of moving average fit (see Materials and Methods section). DNA for this tumor was extracted from a paraffin-embedded specimen, and noise is characteristic. Arrow points to focal amplification on chromosome 1 containing L-Myc. Plots in this format are included in Supplementary Materials (Figure S2) for all specimens.

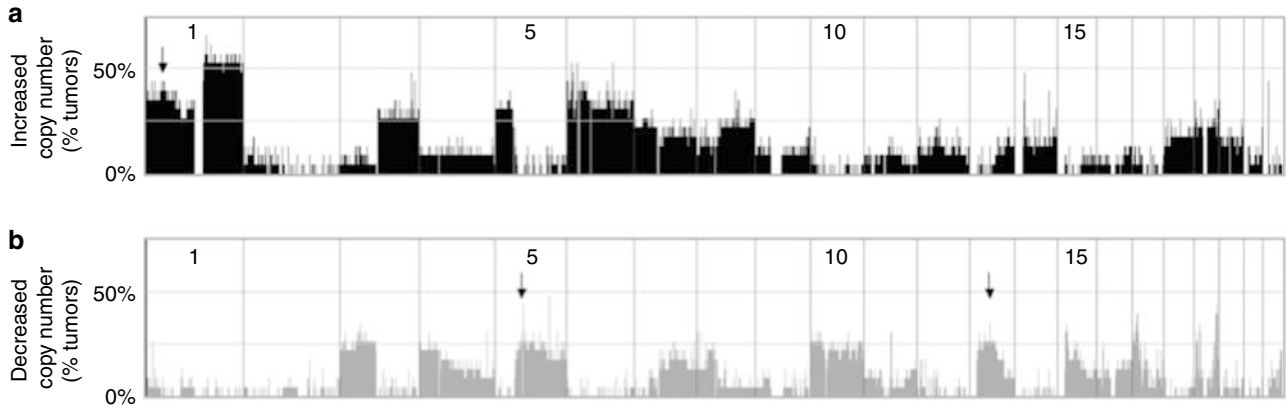


Figure 2. Recurrent changes in relative DNA copy number in 23 Merkel cell carcinomas. The 22 autosomal chromosomes are arranged horizontally along the x-axis, from largest to smallest, with “p” arms to the left. At each genomic location, the percentage of tumors that have an aberration is shown on the y-axis. Significant gains and losses in relative copy number were determined using ACE detection (see Materials and Methods section). (a) Recurrent gains across the genome. The arrow points to the 1p34 amplification detailed in Figure 4. (b) Recurrent losses across the genome. Arrows represent the 5q and 13q deletions detailed in Figure 4. A similar figure in which Merkel cell polyomavirus positive and negative tumors are shown separately is available in Supplementary Materials (Figure S1).

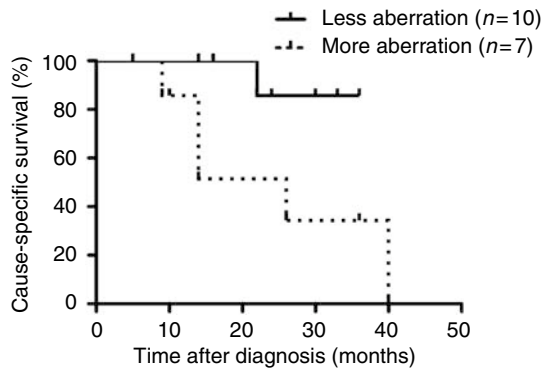


Figure 3. Extent of genomic aberration is associated with disease-specific survival. Survival data was available for 17 patients. This Kaplan–Meier analysis compares disease-specific survival of patients whose tumors displayed less genomic aberration (solid line, <15% of CGH probes aberrant) and those whose tumors displayed more genomic aberration (dotted line, 15% or more probes aberrant). Aberration was defined as a probe being $>2.3n$ or $<1.75n$. Patients with less aberration displayed significantly improved survival, $P=0.04$ by log-rank test.

copy errors analyzed log-ratio values greater than 0.2 or less than -0.2 ($>2.3n$ and $<1.75n$ relative copy number, respectively). We then calculated the percentage of probes that were aberrant for each tumor. It must be noted that the simple calculation of \log_2 ratio to actual copy number does not take into account the small amount of stromal contamination or heterogeneity. However, we feel this approximation is useful as it aids interpretation of our findings.

We observed a wide range of genomic variation between MCC tumors. Three tumors had very high levels of alteration with $>50\%$ probes aberrant, whereas five tumors had almost no detectable copy number alteration with $<5\%$ probes aberrant. Copy number transitions were also determined, and the number of copy number transitions was highly correlated with percentage aberration for any given tumor (data not

shown). Percent aberration and copy number transition are different metrics of overall genome rearrangement. The former estimates the percentage of the overall genome with an aberrant copy number, and the latter gives the average number of chromosomal rearrangements or breaks in a given tumor. The percentage aberration metric was chosen for analysis because a copy number transition analysis scores a narrow region of alteration the same as a wide region and may underrepresent the amount of genomic change.

Disease-specific survival information was available for 17 patients. To investigate whether the percentage of aberrant probes for each tumor was associated with cause-specific survival, tumors were assigned to one of two groups: less aberration (fewer than 15% probes aberrant) or more aberration (15% or more probes aberrant). As shown in Figure 3, less aberration was associated with significantly improved disease-specific survival ($P=0.04$). Less aberration was associated with excellent cause-specific survival whereas outcomes in the more aberration group were mixed. Previous studies have also reported that low aberration in MCC tumors is associated with improved survival (Van Gele *et al.*, 1998; Larramendy *et al.*, 2004); however, this study is the first such association to reach statistical significance.

Three interesting narrow regions of amplification and deletion

Several of the regions of recurrent genomic aberration were especially interesting because they were altered in a substantial portion ($>25\%$) of MCC tumors, were focal enough to contain fewer than 100 annotated genes, and contained biologically plausible known cancer-related genes. Graphical images of these three regions are shown in Figure 4, and accompanying information is in Table 2.

Previous studies have reported that RB1, a well-characterized tumor suppressor, is lost in a subset of MCC tumors (Van Gele *et al.*, 1998). Of 23, 6 tumors in our study had losses of chromosome 13q14-13q21 (Figure 4a).

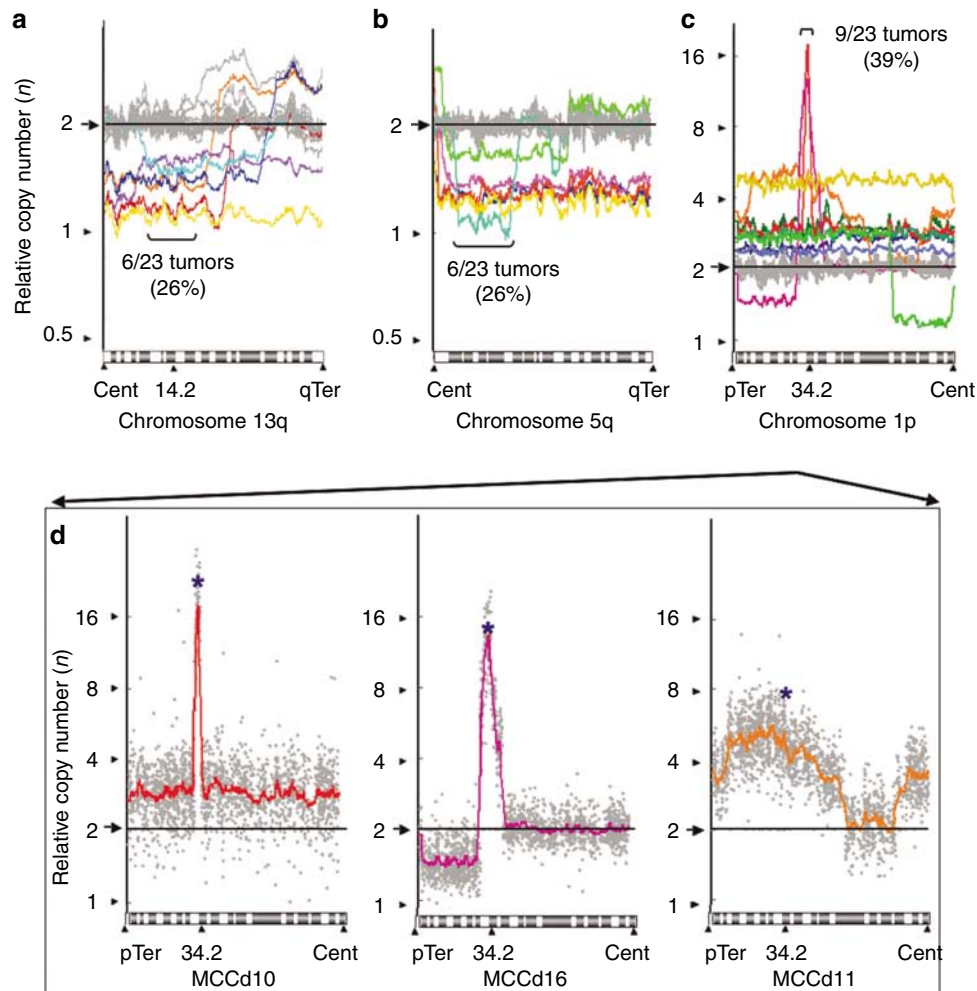


Figure 4. Three narrow regions of recurrent amplification or deletion. Chromosome arms 13q (a), 5q (b), and 1p (c) are shown. These regions were selected because of their high recurrence (>25% of MCCs altered) and focal nature. Colored lines represent individual tumor samples with copy number alteration in the region, and gray lines represent the remaining samples. For further details on these regions see Table 2. (d) Three samples with the highest relative copy number of the 1p34 region are shown in detail. The colored lines are moving average fit lines redrawn from (c), and the gray dots represent individual data points. The probe targeting L-Myc is shown with a blue asterisk. Cent = centromere, pTer = p-terminal, qTer = q-terminal. Note y-axis scale difference between (a) and (b) versus (c).

Table 2. Characteristics of minimum common regions shown in Figure 4

Location of recurrent copy number alteration	Chromosome 13q14.11-13q21.33	Chromosome 5q12.3-5q21.1	Chromosome 1p34.3-1p34.2
Type of alteration	Deletion	Deletion	Amplification
Approximate size (kb)	30,700	34,700	3,400
Tumors with copy number alteration	MCCd1, MCCd16, MCC ₁ 1T, MCC ₁ 3T, MCC ₁ 5T, MCC ₁ 13T	MCCd1, MCCd16, MCC ₁ 1T, MCC ₁ 5T, MCC ₁ 12T, MCC ₁ Sm	MCCd1, MCCd8, MCCd10, MCCd11, MCCd16, MCC ₁ 3T, MCC ₁ 12T, MCC ₁ 16T, MCC ₁ Sm
Number of named genes in region	67	94	29
Genes of interest	<i>RB1, TPT1, RFP2, DLEU1, DLEU2, DLEU7</i>	<i>XRCC4, RASA1</i>	<i>MYCL1, MYCBP, HEYL</i>
Functional RNAs in region	miR-16-1, miR-15a, miR-621, ACA31	miR-9-2, miR-583, HBI-115, U109	miR-30e, miR-30c, ACA55

A list of all annotated genes in each region is included in Table S1.

A region of recurrent deletion was located at chromosome 5q12-21 (Figure 4b). This region was lost in 6 of 23 tumors. A previous study found that this region is also deleted in 71% of BRCA1-mutant breast cancers ($n=42$), which suggests it may contain a tumor suppressor (Johansdottir *et al.*, 2006).

We found a previously unreported recurrent amplification at 1p34 (Figure 4c). The region is amplified in 9 of 23 tumors; two specimens have especially focal amplifications and an average relative copy number of $>10n$. The 1p34 region is gene rich and contains 29 annotated genes including *L-Myc*, a close relative of the protooncogene *c-Myc*. No relationship was observed between these three narrow regions of aberration and the presence of MCPyV DNA.

L-Myc is expressed in MCC tumors

We chose the 1p34 amplification for further analysis because of the focal, high-magnitude copy number increase in a subset of MCC tumors. Among the 29 genes in this region, we focused on the *L-Myc* gene because it is at the center of the peak of the focal amplification (Figure 4d). Furthermore, *L-Myc* is the most biologically plausible candidate oncogene in this region, and it has been implicated as potentially relevant in small cell lung cancer (SCLC), a closely related neuroendocrine tumor (Kim *et al.*, 2006).

Using quantitative PCR, we confirmed the DNA copy number of the *L-Myc* gene in four MCC specimens for which additional FFPE tumor was available (Figure 5a). We further used reverse-transcription PCR to test for RNA expression of *L-Myc*. In a specimen of UV-exposed normal adult skin used as a control, β -actin was expressed but *L-Myc* was undetectable. In contrast, all four MCC tumors expressed both β -actin and *L-Myc* (Figure 5b). Furthermore, the three tumors with gene amplification expressed *L-Myc* RNA in higher levels proportional to their DNA copy number increase.

DISCUSSION

We utilized array-based CGH to generate the most comprehensive overview of genomic aberration in MCC. Among our 25 specimens, the general pattern of recurrence agreed with previous studies with chromosomes 1, 5, 6, and 10 most frequently altered. For the 17 specimens with associated complete survival information, we found a statistically significant association between the amount of genomic aberration and survival. Less aberration was associated with better outcome. This suggests that genomic instability may be involved in the pathogenesis of MCC. There were too few samples, however, to determine prognostic information for individual aberrations. Of the recurrent alterations detected in this study, the most significant is the high amplitude, focal amplification of 1p34. This centers on *L-Myc*, which is a highly plausible oncogene implicated in a closely related neuroendocrine cancer. *L-Myc* RNA expression was increased in proportion to DNA amplification. We anticipate that our complete CGH results, made available in Supplementary Materials, will help inform future studies of neuroendocrine tumors.

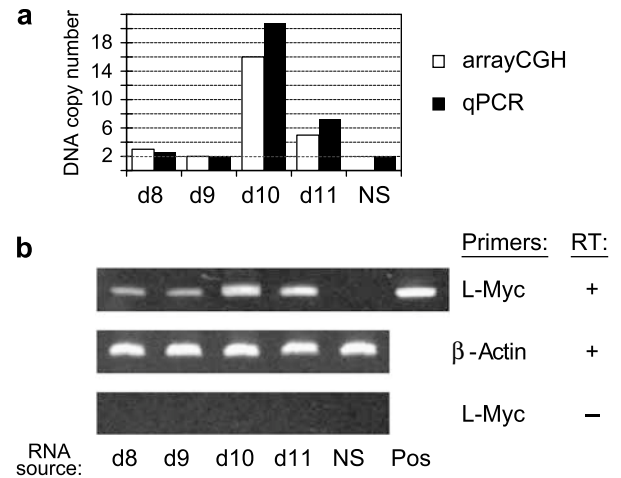


Figure 5. L-Myc DNA amplification and RNA expression in selected MCC tumors. Four tumors with ample remaining materials were chosen for additional analysis. Three of these tumors (MCCd8, MCCd10, MCCd11) had amplification of the *L-Myc* locus by aCGH, and one tumor (MCCd9) had normal, $2n$ copy number at the *L-Myc* locus (Figure 4c). (a) Quantitative PCR confirmation of *L-Myc* DNA copy number amplification. White bars represent copy number determined by array-CGH, and black bars represent copy number as determined by real-time PCR. NS = normal skin (not predicted to have amplification of *L-Myc*). (b) *L-Myc* RNA is expressed in proportion to DNA amplification. *L-Myc* expression was investigated using reverse-transcription PCR. *Top row*: *L-Myc* is expressed in all four studied tumors but not in normal skin. The positive control for *L-Myc* PCR detection (pos) was an *L-Myc* expression construct. *Middle row*: β -Actin served as a positive control. *Bottom row*: As a negative control, the same experiments were performed without reverse-transcriptase (RT). Three reactions were run for all conditions, and the gels shown are representative.

Eight specimens in our study had been previously studied using CGH on metaphase spreads (Van Gele *et al.*, 1998). The array-CGH technology detected several focal regions of copy number change that were previously missed. For example, in sample MCC_L3T, array-CGH newly identified a gain on the terminal of 14q32-14qter that contains *AKT1*, a well-known gene with antiapoptotic functions. In sample MCC_L1T, we found a previously unreported narrow deletion on chromosome 4q21-4q22 that contains a protein phosphatase, *PTPN13*, that acts as a tumor suppressor (Spanos *et al.*, 2008). Further, we found that sample MCC_L12T had a narrow high-magnitude amplification on chromosome 11p13. This region contains only one full gene, *CD44*, which is a cell surface protein involved in hyaluronic acid biology and cell migration/metastasis (Gotte and Yip, 2006; Sackstein *et al.*, 2008). These interesting findings highlight the utility of the detailed data derived from the present array-CGH platform.

The 13q14-13q21 region of recurrent deletion contains the *RB1* gene. Of the six MCC tumors that had deletions in this region, four were previously reported to have this deletion and indeed had lost expression of RB1 protein (Van Gele *et al.*, 1998). Interestingly, the miRNAs miR-16-1 and miR-15a are also located in this portion of chromosome 13. These miRNAs are postulated to act as tumor suppressors by posttranscriptionally downregulating

BCL-2 (Cimmino *et al.*, 2005). Thus the loss of these miRNAs may be linked to BCL-2 upregulation. This is relevant because BCL-2 protein levels are commonly elevated in MCC tumors (Kennedy *et al.*, 1996; Plettenberg *et al.*, 1996), and high BCL-2 levels have been shown to be functionally important in an MCC xenograft model (Schlagbauer-Wadl *et al.*, 2000).

A copy number increase at chromosome 1p34 occurred in 39% of tumors. This previously unreported finding, combined with our RNA expression data, raises the possibility of a role for L-Myc in MCC tumorigenesis. L-Myc is a transcription factor that is closely related to the well-characterized protooncogene *c-Myc* and its homolog *n-Myc* (Nau *et al.*, 1985). The *Myc* genes are basic helix-loop-helix transcriptional regulators. Like *c-Myc* and *n-Myc*, when L-Myc is overexpressed it is able to synergize with Ras to transform fibroblasts in culture. In the cell types tested, L-Myc does so with a reduced efficiency (1–10% of the efficiency of *c-Myc*); however, lines transformed by L-Myc are identical in phenotype and growth rate to those transformed by *c-Myc* overexpression (Birrer *et al.*, 1988).

Unlike the well-characterized *c-Myc* and *n-Myc*, the functional role of L-Myc in human cancer is less well defined. L-Myc was initially discovered in SCLC where it is increased in copy number 10- to 20-fold (Nau *et al.*, 1985). SCLC is a neuroendocrine tumor that shares nearly identical histology with MCC. In several SCLC cell lines with L-Myc amplifications, a reduction of L-Myc expression inhibited cell line growth in a dose-dependent manner (Dosaka-Akita *et al.*, 1995). A recent array-based approach investigated gene amplification and expression profiles in 24 SCLC cell lines (Kim *et al.*, 2006). Of 24, 13 cell lines carried amplifications of *c-Myc*, *n-Myc*, or L-Myc. Interestingly, no cell line carried a DNA amplification of more than one *Myc* gene, suggesting amplification of the various *Myc* genes may be functionally reciprocal. However, expression analysis showed that the downstream effects of *c-Myc*, *n-Myc*, and L-Myc amplification differed, so the exact mechanism of L-Myc oncogenesis remains unclear.

A newly discovered polyomavirus, MCPyV, was recently reported to be associated with MCC tumors (Feng *et al.*, 2008). This virus remains to be functionally characterized but may plausibly contribute to a subset of MCCs because it is predicted to encode two oncogenic proteins (“T antigens”; Garneski *et al.*, 2008a). We tested our samples for the presence or absence of MCPyV DNA (Table 1) and found that samples with detectable viral DNA had fewer deletions than those without (Supplementary Materials, Figure S1). A notable exception is chromosome arm 19q, deleted in the majority of virus positive MCC but rarely deleted in virus negative MCC. The significance of these findings remains unclear, and a more complete analysis of the potential interplay between MCPyV and genomic changes is beyond the scope of this report.

The present array-CGH study of 25 MCC tumors provides insight into genetic aberrations in this poorly understood disease. This high-resolution dataset is made available to the public to help advance studies of this lethal cancer.

Furthermore, these findings suggest an exciting new lead for further study; L-Myc amplification is possibly involved in the pathogenesis of MCC. Future studies are needed to characterize a possible functional role of Myc family members in MCC.

MATERIALS AND METHODS

Patients and tumor samples

In adherence with the Declaration of Helsinki Principles and keeping with National Institutes of Health guidelines for the protection of human subjects, institutional review board approval was obtained from Dana-Farber/Harvard/Partners; patient consent was not required for the use of discarded human tissues. The MCC tumor samples were FFPE archival specimens or flash-frozen surgical tissue. FFPE tumor sections were obtained from Dana-Farber/Brigham and Women’s Cancer Center Pathology or from Cohen Dermatopathology. For two patients, samples of both the primary and metastasis were available (MCCd1p, MCCd1m, MCCd3p, and MCCd3m). Tumor samples with a name containing the letter “L” were provided as DNA extracted from flash-frozen Australian MCC tumor specimens that are previously described (Leonard *et al.*, 1996). MCC diagnoses were made by a dermatopathologist and confirmed with immunohistochemistry and/or with lung imaging to rule out a metastasis originating from a SCLC primary tumor.

DNA and RNA extraction from FFPE tissues

For DNA extraction, 10 μm sections were cut from FFPE blocks containing at least 70% tumor cells as determined by microscopic examination of adjacent sections. Paraffin was removed by sequential xylene and ethanol washes, and the formalin was removed by a phosphate-buffered saline wash (pH 7.2). DNA was purified using a DNeasy Tissue Mini kit (Qiagen, Valencia, CA) and the integrity confirmed by visualization on a 1% agarose gel. RNA was extracted from 5 μm sections of the same block using the RNeasy FFPE kit (Qiagen).

Array-CGH

A total of 15 μg of genomic DNA were digested with AluI and RsaI (New England Biolabs, Ipswich, MA) and purified using the QIAquick PCR Purification kit (Qiagen). DNA was eluted in water and diluted to 100 $\text{ng}\mu\text{l}^{-1}$. DNA was random-prime labeled as described (Aguirre *et al.*, 2004) and hybridized to human 60-mer oligonucleotide microarrays (Agilent, Santa Clara, CA). A single batch of human, male, pooled lymphocyte DNA was used for the reference DNA for all samples (Promega, Madison, WI). Please see the complete description of this hybridization protocol for further details (Protopopov *et al.*, 2008). Samples MCC_L4T, MCC_L12T, MCC_L13T, MCC_L21T, and MCC_LSm were run on G4410B chip and the remainder were run on the G4410A chip. The microarrays contain over 40,000 coding and noncoding sequences, and provide 43 kb overall median resolution, which improves to a resolution of 24 kb in gene rich regions. The fluorescence ratios for samples MCCd1p, MCCd3p-MCCd16, MCC_L1T, MCC_L3T, MCC_L5T, and MCC_L16T were calculated using the average of two paired (dye swap) arrays. The fluorescence ratios for tumor samples MCCd1m, MCC_L4T, MCC_L12T, MCC_L13T, MCC_L21T, and MCC_LSm were calculated using a single dye array; this was feasible because of higher DNA quality from the frozen tissues.

Detection of Merkel cell polyomavirus

Tumor specimens were tested for the presence of MCPyV DNA by real-time PCR as described (Garneski *et al.*, 2008b). One specimen was not available for testing because of insufficient sample volume. The viral status of 14 of these samples were previously reported (Garneski *et al.*, 2008b).

Quantitative PCR

Confirmation of L-Myc copy number was performed by real-time quantitative PCR. Primers were designed to amplify L-Myc and control genomic DNA sequences. The control sequence was selected within a region of euploid copy number on chromosome 2 (near the *TPO* gene). A total of 2.5 ng of DNA were combined with primers and 2 × SYBR green PCR mastermix (Applied Biosystems, Foster City, CA), denatured at 95 °C for 10 minutes, and then run for 40 cycles of 95 °C for 15 seconds followed by 1 minute of annealing at 60 °C. Fluorescence was detected using an Applied Biosystems 7900 HT sequence detection system, and relative quantities were determined using the comparative C_t ($\Delta\Delta C_t$) method as described by the manufacturer. DNA from FFPE sun exposed, disease free, normal human skin was used as a control for copy number, and water served as a negative control. Copy number was compared to the moving average fit values for 1p34 (Figure 4c). All wells were run in triplicate, and the experiment was repeated twice. Several genomic sequences located on chromosomes 1, 3, 10, and 14 were also studied to confirm validity of CGH results, and all were consistent with CGH findings (data not shown). Primer sequences are as follows: control (*TPO*) forward AACCTCCTGAGCCAACAAGC and reverse CACACATTACCCGTTGGATG (expected product length 127 bp), L-Myc forward CAGTGAGCTTCTTGGTCCT and reverse TGGCATCTTAGACCTCCACA (expected product length 105 bp).

Reverse-transcription PCR

The high capacity cDNA reverse-transcription kit (Applied Biosystems) was used with random primers to reverse transcribe 0.5 µg of total RNA. Primers were designed to β-actin (PCR control) and L-Myc. Forward and reverse primers were designed to span exons so as to only amplify cDNA. In addition, the same experiments were repeated without reverse transcriptase as a negative control. cDNA was amplified with 38 cycles of PCR (95 °C for 15 seconds then 60 °C for 1 minute); the product was visualized on an 8% acrylamide Tris borate EDTA gel stained with ethidium bromide. One picogram of a plasmid containing full length L-Myc cDNA was used as the positive control. We were unable to assay levels of L-Myc protein because no adequate antibody is commercially available. Primer sequences are as follows: control (β-actin) forward AGAGCTACGAGCTGCCTGAC and reverse AAGGTAGTTTCGTGGATGCC (expected product length 129 bp), L-Myc forward AGCGACTCGGAGAATGAAGA and reverse CAGCTTCTGGAGGAAAACG (expected product length 180 bp).

Statistical analysis

Array data was log transformed and mode centered. The CGH-Explorer program (version 3.1; Lingjaerde *et al.*, 2005) was used to visualize and analyze the CGH data. Genome-wide profile images displaying the raw data for each sample were plotted, and a “moving average fit” line was applied to each image (neighborhood size = 29). Images for each sample are included in Supplementary

Materials (Figure S2). Views of the minimum common regions for Figure 4 were also generated using moving average fit; individual data points were not displayed for (a), (b), and (c), and the neighborhood size was increased to 39 to better enable visualization of multiple samples on the same graph. Statistically significant copy number alterations were identified by applying the analysis of copy errors detection algorithm (Lingjaerde *et al.*, 2005), which is a validated algorithm used to determine regions of loss and gain (Meza-Zepeda *et al.*, 2006). Data from the 22 autosomal chromosomes were analyzed. Sex chromosomes were excluded because of gender differences between patients. The stringent cutoff of the false discovery rate was set at 0.003, indicating three probes per 1,000 were falsely called aberrant. The terms “copy number gain” and “amplification” are used synonymously in this paper to denote a DNA gain. Raw array data and complete analysis results are included in Supplementary Materials and will be posted at the Progenetix online resource (www.progenetix.net) and at the NCI and NCBI's Raw array data and complete analysis results are included in Supplementary Materials and will be posted at the Progenetix online resource (www.progenetix.net) and at the NCI and NCBI's GEO Database (<http://www.ncbi.nlm.nih.gov/geo/>). Annotated genes within the three narrow regions of recurrent aberration (Figure 4 and Table 2) were identified using the Santa Cruz Genome Browser. Kaplan–Meier curves were generated using GraphPad Prism, version 5 (GraphPad Software, San Diego, CA).

CONFLICT OF INTEREST

The authors state no conflict of interest.

ACKNOWLEDGMENTS

We thank the Bomszyk Lab at the University of Washington for advice and reagents and the Eisenman Lab at the Fred Hutchinson Cancer Research Center for the gift of an L-Myc plasmid. Array-CGH profiling was performed at the Belfer Center for Cancer Genomics in the Center for Applied Cancer Science at Dana-Farber Cancer Institute. This project was supported by the Harvard Skin Cancer SPORE, NIH-K02-AR050993, the American Cancer Society Jerry Wachter Fund for MCC Research, the Skin Cancer Foundation, and the MCC Patient Gift Fund at the University of Washington.

SUPPLEMENTARY MATERIAL

Table S1. Full list of named genes from minimum common regions in Table 2.

Figure S1. Recurrent changes in relative DNA copy number in Merkel cell carcinomas with and without detectable Merkel cell polyomavirus (MCPyV).

Figure S2. Genome-wide profiles of Merkel cell carcinoma tumors studied.

Array CGH Data File. Log base 2 transformed and Analysis of Copy Error (ACE) analyzed CGH data (txt file).

REFERENCES

- Aguirre AJ, Brennan C, Bailey G, Sinha R, Feng B, Leo C *et al.* (2004) High-resolution characterization of the pancreatic adenocarcinoma genome. *Proc Natl Acad Sci USA* 101:9067–72
- Allen PJ, Bowne WB, Jaques DP, Brennan MF, Busam K, Coit DG (2005) Merkel cell carcinoma: prognosis and treatment of patients from a single institution. *J Clin Oncol* 23:2300–9
- American Cancer Society (2006) *Cancer Facts and Figures 2006*. Atlanta: American Cancer Society: 2006.
- Birrer MJ, Segal S, DeGreve JS, Kaye F, Sausville EA, Minna JD (1988) L-myc cooperates with ras to transform primary rat embryo fibroblasts. *Mol Cell Biol* 8:2668–73
- Boulais N, Misery L (2007) Merkel cells. *J Am Acad Dermatol* 57: 147–165

- Brennan C, Zhang Y, Leo C, Feng B, Cauwels C, Aguirre AJ *et al.* (2004) High-resolution global profiling of genomic alterations with long oligonucleotide microarray. *Cancer Res* 64:4744–8
- Cimmino A, Calin GA, Fabbri M, Iorio MV, Ferracin M, Shimizu M *et al.* (2005) Mir-15 and mir-16 induce apoptosis by targeting bcl2. *Proc Natl Acad Sci USA* 102:13944–9
- Dosaka-Akita H, Akie K, Hiroumi H, Kinoshita I, Kawakami Y, Murakami A (1995) Inhibition of proliferation by L-Myc antisense DNA for the translational initiation site in human small cell lung cancer. *Cancer Res* 55:1559–64
- Feng H, Shuda M, Chang Y, Moore PS (2008) Clonal integration of a polyomavirus in human Merkel cell carcinoma. *Science* 319:1096–100
- Garneski KM, Decaprio JA, Nghiem P (2008a) Does a new polyomavirus contribute to Merkel cell carcinoma? *Genome Biol* 9:228
- Garneski KM, Warcola AH, Feng Q, Kiviat NB, Leonard JH, Nghiem P (2008b) Merkel cell polyomavirus is more frequently present in North American than Australian Merkel cell carcinoma tumors. *J Invest Dermatol*, E-pub ahead of print July 24, 2008.
- Gotte M, Yip GW (2006) Heparanase, hyaluronan, and cd44 in cancers: a breast carcinoma perspective. *Cancer Res* 66:10233–7
- Haeberle H, Fujiwara M, Chuang J, Medina MM, Panditrao MV, Bechstedt S *et al.* (2004) Molecular profiling reveals synaptic release machinery in Merkel cells. *Proc Natl Acad Sci USA* 101:14503–8
- Harle M, Arens N, Moll I, Back W, Schulz T, Scherthan H (1996) Comparative genomic hybridization (CGH) discloses chromosomal and subchromosomal copy number changes in Merkel cell carcinomas. *J Cutan Pathol* 23:391–7
- Heath M, Jaimes N, Lemos B, Mostaghimi A, Wang LC, Penas PF *et al.* (2008) Clinical characteristics of Merkel cell carcinoma at diagnosis in 195 patients: the AEIOU features. *J Am Acad Dermatol* 58:375–81
- Hodgson NC (2005) Merkel cell carcinoma: changing incidence trends. *J Surg Oncol* 89:1–4
- Houben R, Michel B, Vetter-Kauczok CS, Pfohler C, Laetsch B, Wolter MD *et al.* (2006) Absence of classical map kinase pathway signalling in Merkel cell carcinoma. *J Invest Dermatol* 126:1135–42
- Johannsdottir HK, Jonsson G, Johannsdottir G, Agnarsson BA, Eerola H, Arason A *et al.* (2006) Chromosome 5 imbalance mapping in breast tumors from brca1 and brca2 mutation carriers and sporadic breast tumors. *Int J Cancer* 119:1052–60
- Kennedy MM, Blessing K, King G, Kerr KM (1996) Expression of bcl-2 and p53 in Merkel cell carcinoma. An immunohistochemical study. *Am J Dermatopathol* 18:273–7
- Kim YH, Girard L, Giacomini CP, Wang P, Hernandez-Boussard T, Tibshirani R *et al.* (2006) Combined microarray analysis of small cell lung cancer reveals altered apoptotic balance and distinct expression signatures of myc family gene amplification. *Oncogene* 25:130–8
- Larramendy ML, Koljonen V, Bohling T, Tukiainen E, Knuutila S (2004) Recurrent DNA copy number changes revealed by comparative genomic hybridization in primary Merkel cell carcinomas. *Mod Pathol* 17:561–7
- Lemos B, Nghiem P (2007) Merkel cell carcinoma: more deaths but still no pathway to blame. *J Invest Dermatol* 127:2100–3
- Leonard JH, Williams G, Walters MK, Nancarrow DJ, Rabbitts PH (1996) Deletion mapping of the short arm of chromosome 3 in Merkel cell carcinoma. *Genes Chromosomes Cancer* 15:102–7
- Lingjaerde OC, Baumbusch LO, Liestol K, Glad IK, Borresen-Dale AL (2005) CGH-Explorer: a program for analysis of array-CGH data. *Bioinformatics* 21:821–2
- Liu S, Daa T, Kashima K, Kondoh Y, Yokoyama S (2007) The wnt-signaling pathway is not implicated in tumorigenesis of Merkel cell carcinoma. *J Cutan Pathol* 34:22–6
- Meza-Zepeda LA, Kresse SH, Barragan-Polania AH, Bjerkehegen B, Ohnstad HO, Namlos HM *et al.* (2006) Array comparative genomic hybridization reveals distinct DNA copy number differences between gastrointestinal stromal tumors and leiomyosarcomas. *Cancer Res* 66:8984–93
- Nau MM, Brooks BJ, Battey J, Sausville E, Gazdar AF, Kirsch IR *et al.* (1985) L-myc, a new myc-related gene amplified and expressed in human small cell lung cancer. *Nature* 318:69–73
- Plettenberg A, Pammer J, Tschachler E (1996) Merkel cells and Merkel cell carcinoma express the bcl-2 proto-oncogene. *Exp Dermatol* 5: 183–188
- Popp S, Waltering S, Herbst C, Moll I, Boukamp P (2002) Uv-b-type mutations and chromosomal imbalances indicate common pathways for the development of Merkel and skin squamous cell carcinomas. *Int J Cancer* 99:352–60
- Protopopov A, Feng B, Chin L (2008) Full complexity genomic hybridization on 60-mer oligonucleotide microarrays for array comparative genomic hybridization (ACGH). In: *Genomics Protocols: Second edition, Methods in Molecular Biology*. (Starkey M, Elaswarapu R, eds) Humana Press Inc.: Totowa, NJ, 87–100
- Sackstein R, Merzaban JS, Cain DW, Dagia NM, Spencer JA, Lin CP *et al.* (2008) Ex vivo glycan engineering of cd44 programs human multipotent mesenchymal stromal cell trafficking to bone. *Nat Med* 14:181–7
- Schlagbauer-Wadl H, Klosner G, Heere-Ress E, Waltering S, Moll I, Wolff K *et al.* (2000) Bcl-2 antisense oligonucleotides (g3139) inhibit Merkel cell carcinoma growth in scid mice. *J Invest Dermatol* 114:725–30
- Spanos WC, Hoover A, Harris GF, Wu S, Strand GL, Anderson ME *et al.* (2008) The pdz binding motif of human papillomavirus type 16 e6 induces ptpn13 loss, which allows anchorage-independent growth and synergizes with ras for invasive growth. *J Virol* 82: 2493–2500
- Swick BL, Ravel L, Fitzpatrick JE, Robinson WA (2007) Merkel cell carcinoma: evaluation of kit (cd117) expression and failure to demonstrate activating mutations in the c-kit proto-oncogene—implications for treatment with imatinib mesylate. *J Cutan Pathol* 34:324–9
- Tonon G, Wong KK, Maulik G, Brennan C, Feng B, Zhang Y *et al.* (2005) High-resolution genomic profiles of human lung cancer. *Proc Natl Acad Sci USA* 102:9625–30
- Van Gele M, Kaghad M, Leonard JH, Van Roy N, Naeyaert JM, Geerts ML *et al.* (2000) Mutation analysis of p73 and tp53 in Merkel cell carcinoma. *Br J Cancer* 82:823–6
- Van Gele M, Leonard JH, Van Roy N, Van Limbergen H, Van Belle S, Cocquyt V *et al.* (2002) Combined karyotyping, CGH and m-fish analysis allows detailed characterization of unidentified chromosomal rearrangements in Merkel cell carcinoma. *Int J Cancer* 101:137–45
- Van Gele M, Speleman F, Vandesompele J, Van Roy N, Leonard JH (1998) Characteristic pattern of chromosomal gains and losses in Merkel cell carcinoma detected by comparative genomic hybridization. *Cancer Res* 58:1503–8